Electronic Supplementary Material (ESI) for Chemical Communications

Electronic Supporting Information for "Indirect and Direct ^{29}Si Dynamic Nuclear Polarization of Dispersed Nanoparticles"

Olivier Lafon,*[a] Aany Sofia Lilly Thankamony,[a] Melanie Rosay,[b]
Fabien Aussenac,[c] Xingyu Lu,[a]
Julien Trébosc,[a] Viviane Bout-Roumazeilles,[d]
Hervé Vezin,[e] and Jean-Paul Amoureux[a]

[a] Univ. Lille Nord de France; CNRS, UMR 8181 – UCCS;
Univ. Lille 1, F-59652 Villeneuve d'Ascq, France
E-mail: olivier.lafon@univ-lille1.fr

[b] Bruker Biospin Corporation, 15 Fortune Drive, Billerica, MA 01821, USA

[c] Bruker Biospin SA, 34, rue de l'Industrie, 67166 Wissembourg Cedex, France

[d] Univ. Lille Nord de France, CNRS, UMR 8217, Géosystèmes;
Univ. Lille 1, Bât. SN5, F-59652 Villeneuve d'Ascq, France

[e] Univ. Lille Nord de France, CNRS, UMR 8516 – LASIR;
Univ. Lille 1, Bât. C4, F-59652 Villeneuve d'Ascq, France

November 29, 2012

Sample preparation

The laponite® RD (**1**) was purchased from Rockwood Additives Ltd., Widnes (UK). It is a trioctahedral 2:1 phyllosilicate with the empirical formula $Na_{0.7}[Si_8Mg_{5.5}Li_{0.3}O_{20}(OH)_4]$. Samples for solid-state DNP NMR experiments were prepared by dispersing at room temperature (20 °C) about 100 mg of **1** in about 340 mg of 20 mM TOTAPOL[1] solution in $[^2H_6]$-DMSO/^2H_2O/H_2O mixture (78/14/8 w/w/w). The mixture was stirred vigorously until the formation of a viscous, translucent and yellowish gel.

The bentonite (**2**) is taken from an Oxfordian (Upper Jurassic) deposit in Paris bassin and primarily consists of montmorillonite, a dioctahedral 2:1 phyllosilicate. **2** may also contain traces of feldspar, quartz, calcite, and gypsum. The empirical formula of **2** is $Ca_{0.2}(Al,Mg)_2Si_4O_{10}(OH)_2$-$4H_2O$. In **2**, the montmorillonite platelets exhibit a uniform height of 1 nm, whereas they vary in both shape and size. The longest chord inside the platelet ranges from 5 to 750 nm and its average value is about 300 nm.[2,3] Samples for solid-state DNP NMR experiments were prepared by dispersing about 100 mg of **2** in about 290 mg of 20 mM TOTAPOL solution in $[^2H_6]$-DMSO/^2H_2O/H_2O mixture (78/14/8 w/w/w). **2** and the solution were stirred vigorously until the formation of a colloidal suspension. After three days, the sample was centrifuged during 5 min at a relative centrifugal force of 12,110 to remove the excess of solution.

The impregnated samples were placed into a 3.2 mm sapphire rotors for DNP experiments.

EPR experiments

X-band EPR experiments were performed using a Bruker Biospin ELEXYS E580E spectrometer. The spectra were recorded with respectively 2 mW microwave power and 0.5 G of amplitude modulation. Spin concentration of sample was determined by full spectra integration.

Figure S1a shows the EPR spectrum of **1**. The signal-to-noise ratio of this spectrum is close to 2 and hence the concentration of electron spins, c_e[spins.g^{-1}], expressed in spins.g^{-1}, is comparable to the lower limit of detection of the EPR spectrometer, i.e. 10^{13} spins.g^{-1}. The concentration of electron spins, c_e[M], expressed in M, is

$$c_e[\mathrm{M}] = \frac{10^3 c_e[\mathrm{spins.g^{-1}}]\rho_b}{N_A} \approx 2 \times 10^{-8}\ \mathrm{M} \qquad \text{(S1)}$$

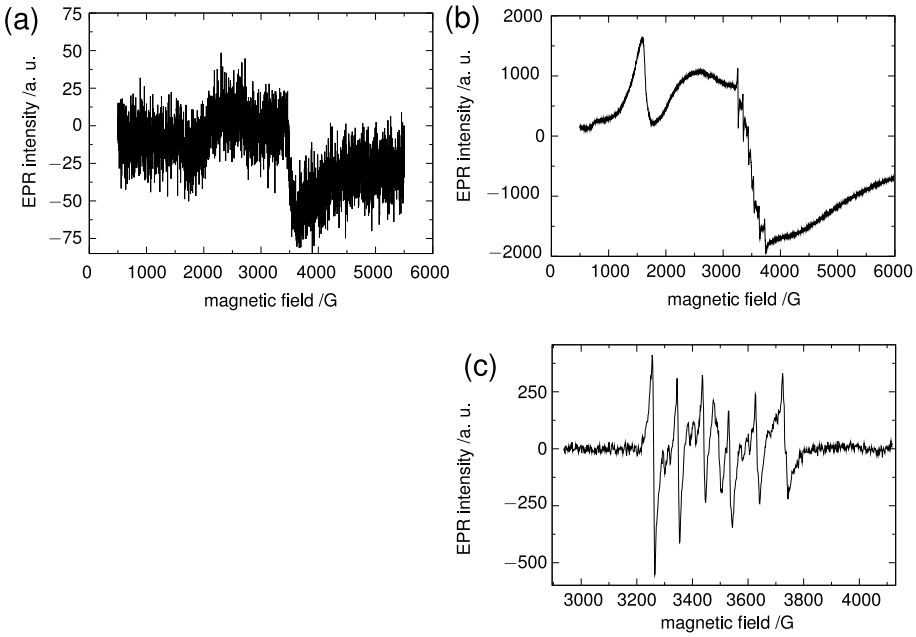

Figure S1: 9 GHz continuous wave EPR spectra of (a) **1** and (b-c) **2**. The spectrum c is an expansion of spectrum b, centered on the signal of the Mn(II) sites. The spectra were recorded at room temperature and the samples were powders. The EPR intensities are expressed in an arbitrary unit, which is identical for the three spectra.

where $\rho_b \approx 1$ kg.dm^{-3} is the bulk density of **1** and N_A is the Avogadro number.

In Figure S1b, the narrow resonance centered about $g \approx 4.3$ was attributed to octahedrally coordinated high spin ($S = 5/2$) Fe(III) atoms, which substitute Al(III) atoms in the octahedral layer of montmorillonite.[4,5] The broad resonance ($\Delta B > 10^3$ G) at about $g \approx 2$ stems from iron (III) oxides which are often present in **2** ores.[4,5] The concentration of electron spins for iron oxide was estimated to be in the order of 10^{17} spins g^{-1}. However, the unpaired electrons in iron oxide are submitted to ferromagnetic interactions, which can bias the measurement of electron spin density. In addition, narrow resonances are superimposed to the iron oxide signal. An expansion of these resonances after baseline correction is shown in Figure S1c. This spectrum is a powder lineshape centered at $g \approx 2$, which consists of six intense resonances and weaker doublets, which appear between the intense resonances. These spectral features are characteristic of high-spin ($S = 5/2$) Mn(II) sites with axial symmetry.[6] The splitting in six resonances results from anisotropic hyperfine coupling with ^{55}Mn nucleus of nuclear spin $I = 5/2$, whereas the weak doublets stem from forbidden hyperfine transitions corresponding to the changes, $\Delta m_S = \pm 1$ and $\Delta m_I = \pm 1$, in the azimuthal quantum numbers of the unpaired electron and ^{55}Mn nucleus. The Mn(II) sites in montmorillonite were ascribed to interlayer Mn(II) ions.[6] The density of electron spins corresponding to Mn(II) sites was determined using $MnCl_2$ as a reference and is equal to 2.6×10^{16} spins g^{-1}.

DNP experiments

All solid-state DNP MAS experiments were performed on a commercial Bruker BioSpin Avance III DNP spectrometer operating at a microwave frequency of 263 GHz and a ^{29}Si frequency of 79.2 MHz.[7] The wide-bore 9.4 T NMR magnet was equipped with a double resonance ^{1}H/X 3.2 mm low-temperature probe. The sample was placed in a 3.2 mm sapphire rotor. DNP experiments are usually performed at cryogenic temperatures because electron and nuclear relaxation processes slow with decreasing temperature.[7,8] Sample temperature of 98 K was achieved and controlled under MAS condition using a Bruker BioSpin low-temperature MAS cooling system. The sample temperature corresponds to the calibrated temperature with microwave off. During the DNP MAS experiment, a gyrotron generated continuous microwave irradiation, which was delivered to the sample by a corrugated

waveguide. The microwave power at the position of the sample was approximately 6 W. The NMR spectra were recorded at $\nu_r = 8$ kHz and result from averaging 8 transients. A SPINAL-64 decoupling with ^{1}H radiofrequency (rf) nutation frequency of 100 kHz was applied during the acquisition.[9] The indirect DNP ^{29}Si NMR spectra were recorded using a CP-MAS pulse sequence (see Figure S2a) in order to transfer the DNP-enhanced ^{1}H polarization to the ^{29}Si nuclei.[10,11] The indirect DNP ^{29}Si NMR experiments used a microwave polarization time, $\tau_{\mu w} = 5$ s, a ^{1}H 90° pulse length of 2.5 μs, a contact time of 2 ms, a constant ^{29}Si rf nutation frequency of 50 kHz and a linear ramp of ^{1}H rf nutation frequency between 30 kHz and 33 kHz. The direct DNP ^{29}Si NMR spectra were recorded using a ^{29}Si 90° pulse length of 4.2 μs and background suppression (see Figure S2b).[12] Furthermore, the background ^{29}Si signal of the probe was carefully subtracted by recording the DNP ^{29}Si NMR spectra of the empty rotor under identical experimental conditions. In direct ^{29}Si DNP experiments, the equilibrium ^{29}Si Boltzmann was eliminated by a presaturation, consisting of a train of hundred 90° pulses, separated by a delay of $\tau_{ps} = 60$ μs. The ^{29}Si chemical shifts are referenced to tetramethylsilane using the shielded resonance (−9.8 ppm) in the ^{29}Si NMR spectrum of tetrakis(trimethylsilyl)silane as a secondary reference.

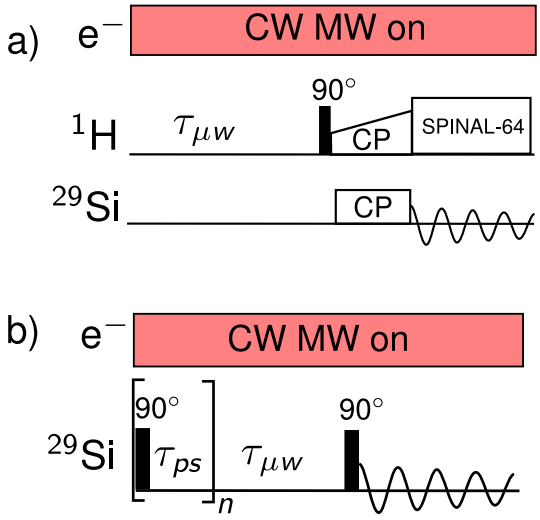

Figure S2: (a) Pulse sequence used for 1D indirect DNP MAS experiment. The longitudinal ^{1}H polarization develops during $\tau_{\mu w}$ and is finally transferred to ^{29}Si nuclei using a CP step. (b) Pulse sequence used for 1D direct DNP MAS experiment. The longitudinal ^{29}Si polarization builds up during the microwave polarization time, $\tau_{\mu w}$. The same experiment without microwave irradiation serves as a reference for the measurement of signal enhancement by direct DNP.

Location of Q^2 sites

We assume that (i) the silicon atoms are located on the lattice points of a hexagonal two-dimensional lattice, (ii) the NP has the shape of a regular hexagon, (iii) the silicate sites at the edge of the NP are Q^2 sites. This type of structure is depicted in Figure S3. Under these assumptions and taking into the account the two silicate disks in **1** NP, the numbers of Q^2 sites at the NP edges, $N(Q^{2\text{edge}})$, and of internal silicon atoms, $N(Q^{\text{int}})$, not located on the edges are

$$N(Q^{2\text{edge}}) = 12k \tag{S2}$$

and

$$N(Q^{\text{int}}) = 12k(k-1) \tag{S3}$$

respectively. The index k denotes the number of concentric siloxane rings. It increases from the center to the periphery of the NP. Therefore, we have

$$\frac{N(Q^{2\text{edge}})}{N(Q^{\text{int}})} = \frac{1}{k-1} \tag{S4}$$

Furthermore, the upper and lower bounds for the diameter, d, of the NP are

$$2\sqrt{3}ka \leq d \leq 4ka \tag{S5}$$

where a is the edge length of silicate tetrahedron and $2\sqrt{3}ka$ and $4ka$ are the diameters of the inscribed and circumscribed circles, respectively (see Figure S3). In the crystal structure of talc, which is structurally related to **1**, the length a varies between 2.64 and 2.66 Å.[13] Similar range for a is expected in **1**. Furthermore, using small-angle X-ray scattering and small-angle neutron scattering, the diameter of **1** nanodisks has been found in the range 25–30 nm.[14,15] Therefore, it can be deduced from Eq. S5 that the k value is in the range 24–32 and hence from Eq. S4, we have

$$\frac{N(Q^{2\text{edge}})}{N(Q^{\text{int}})} < 0.04. \tag{S6}$$

The above equation shows that the ratio $N(Q^{2\text{edge}})/N(Q^{\text{int}})$ differs from the ratio of integrals $r^A = A(Q^2)/A(Q^3) = 0.08$ in the quantitative 1D ^{29}Si NMR spectrum [not shown]. Consequently, the internal silicon atoms are not all Q^3 sites and there must be internal Q^2 sites. The number of internal Q^2

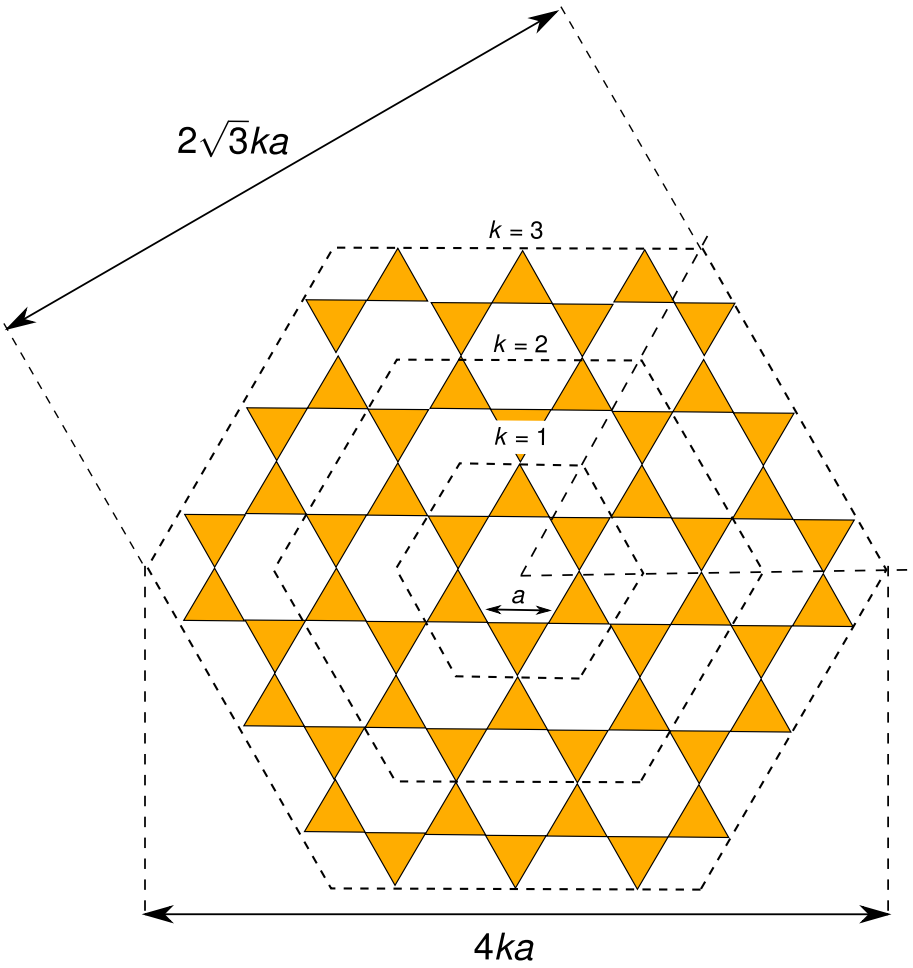

Figure S3: Silicate framework of the tetrahedral sheet in a NP of **1**. The plane of the figure corresponds to the plane of the tetrahedral sheet. The triangles are the bases of silicate tetrahedra.

sites, $Q^{2\mathrm{int}}$, can be estimated from the k and r^A values by solving the system of linear equations, including Eqs. S2 and S3, and the following ones

$$N(Q^2) = N(Q^{2\mathrm{edge}}) + N(Q^{2\mathrm{int}}) \tag{S7}$$

where $N(Q^2)$ is the total number of Q^2 sites in one NP of **1**,

$$N(Q^{\mathrm{int}}) = N(Q^{2\mathrm{int}}) + N(Q^3) \tag{S8}$$

where $N(Q^3)$ is the number of Q^3 sites in one NP of **1**,

$$N(\mathrm{Si}) = N(Q^2) + N(Q^3) \tag{S9}$$

where $N(\mathrm{Si})$ is the number of silicon atom in one NP of **1**,

$$\frac{N(Q^2)}{N(Q^3)} = r^A. \tag{S10}$$

The expressions of $N(Q^{2\mathrm{int}})$ and $N(\mathrm{Si})$ derived from the above equations are

$$N(Q^{2\mathrm{int}}) = 12k\frac{(k-1)r^A - 1}{r^A + 1} \tag{S11}$$

and

$$N(\mathrm{Si}) = 12k^2, \tag{S12}$$

respectively. Consequently, the $N(Q^{2\mathrm{int}})$ value ranges from 228 to 533, whereas the $N(\mathrm{Si})$ value ranges from 3450 to 6150, depending on the diameter of the **1** NP. According to the empirical formula of **1**, the number of Li atoms ranges from 130 for $N(Q^{2\mathrm{int}}) = 228$ to 230 for $N(Q^{2\mathrm{int}}) = 533$ and hence there are about two Q^2 sites for each Li atom. The presence of the internal Q^2 sites might be related to the substitution of Mg^{2+} by Li^+. Furthermore, the amount of internal Q^2 sites is estimated at about 44–58% of the total number of Q^2 sites and at about 6.6–8.7% of the total number of silicon atom in **1**. These estimates agree with the amount of Q^2 sites that do not react during the functionalization of **1** with organic molecules.[16,17] Additional experiments and first-principle calculations will be required to determine the exact structure of the internal Q^2 sites.

Comparison of ^{29}Si NMR spectra enhanced by direct and indirect DNP

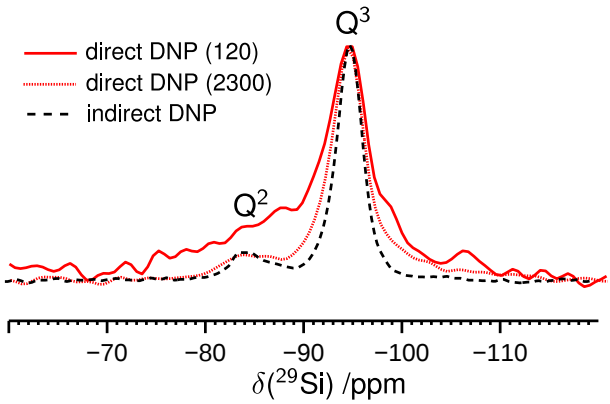

Figure S4: Natural abundance ^{29}Si NMR spectra of **1** obtained via indirect DNP and direct DNP with $\tau_{\mu w} = 120$ s [direct DNP (120)] or 2300 s [direct DNP (2300)]. The indirect and direct DNP (120) spectra are identical to those of Figure 2, but they are scaled to the same absolute intensity in order to show the broadening of ^{29}Si NMR signal in direct DNP experiments. The fullwidth half-height (FWHH) of Q^3 site is 440 Hz in the direct DNP with $\tau_{\mu w} = 120$ s and 300 Hz with $\tau_{\mu w} = 2300$ s, whereas it is 250 Hz in spectrum enhanced by indirect DNP.

Estimate of transfer depth in direct ^{29}Si DNP

We show below that the transfer depth of direct ^{29}Si DNP can be estimated from the fullwidth at half height (FWHH) of Q^3 signals. The ^{29}Si transverse relaxation rate, $1/T_2(^{29}\mathrm{Si})$, governed by ^{29}Si-TOTAPOL interactions represents a lower bound for FWHH. Hence, assuming an exponential decay of the ^{29}Si NMR signal, we have

$$\mathrm{FWHH} \geq \frac{1}{\pi T_2(^{29}\mathrm{Si})}. \tag{S13}$$

The $T_2(^{29}\mathrm{Si})$ relaxation of Q^3 contributing to FWHH is governed by the fluctuations of the dipolar interactions between ^{29}Si and TOTAPOL[18] since (i) in solids, the Curie relaxation[19] is absent[20], (ii) the contact relaxation[21] only dominates for nuclei at a distance shorter than 4 Å from the unpaired electrons[22] and (iii) at MAS frequency of 8 kHz, the signal of nuclei at a distance of few angstroms from the TOTAPOL is quenched by electron-nucleus interactions.[23] Assuming that the point-dipole-approximation holds for the TOTAPOL-^{29}Si interaction and that the electron g-tensor is isotropic, the $1/T_2(^{29}\mathrm{Si})$ rate via electron-nucleus dipolar interactions is given by[18,24,25,19,22]

$$\frac{1}{T_2(^{29}\mathrm{Si})} = \frac{S\,(S+1)}{15}\left[\frac{\mu_0}{4\pi}\frac{\hbar\gamma(^{29}\mathrm{Si})\gamma_e}{r^3}\right]^2\left[4T_{1e} + \frac{3T_{1e}}{1+\omega^2(^{29}\mathrm{Si})T_{1e}^2} + \frac{6T_{2e}}{1+\omega_e^2T_{2e}^2} + \frac{T_{2e}}{1+[\omega(^{29}\mathrm{Si})-\omega_e]^2T_{2e}^2} + \frac{6T_{2e}}{1+[\omega(^{29}\mathrm{Si})+\omega_e]^2T_{2e}^2}\right], \tag{S14}$$

where μ_0 is the magnetic constant, $\hbar$ is the reduced Planck constant, γ_e and $\gamma(^{29}\mathrm{Si})$ are the gyromagnetic ratios of electron and ^{29}Si nucleus, S is the effective spin number for TOTAPOL, which is 1/2 or 1 depending on the coupling between the two unpaired electron, r is the TOTAPOL-^{29}Si distance, T_{1e} and T_{2e} times are the longitudinal and transverse electron relaxation times, $\omega(^{29}\mathrm{Si})$ and ω_e are the ^{29}Si and electron Larmor frequencies. As $\omega(^{29}\mathrm{Si}) = 79.4$ MHz $\ll \omega_e = 263$ GHz, Eq. S14 can be recast as[19,22]

$$\frac{1}{T_2(^{29}\mathrm{Si})} = \frac{S\,(S+1)}{15}\left[\frac{\mu_0}{4\pi}\frac{\hbar\gamma(^{29}\mathrm{Si})\gamma_e}{r^3}\right]^2\left[4T_{1e} + \frac{3T_{1e}}{1+\omega^2(^{29}\mathrm{Si})T_{1e}^2} + \frac{13T_{2e}}{1+\omega_e^2T_{2e}^2}\right]. \tag{S15}$$

The combination of Eqs. S13 and S15 yields a lower bound for r

$$r \geq \left\{ \frac{S\,(S+1)}{15} \left[\frac{\mu_0}{4\pi} \hbar\gamma(^{29}\mathrm{Si})\gamma_e \right]^2 \frac{1}{\pi \mathrm{FWHH}} \times \left[4T_{1e} + \frac{3T_{1e}}{1+\omega^2(^{29}\mathrm{Si})T_{1e}^2} + \frac{13T_{2e}}{1+\omega_e^2 T_{2e}^2} \right] \right\}^{1/6} . \tag{S16}$$

The right member of the above equation depends on the electron relaxation times. EPR measurements at $B^0 = 3.35$ T on TOTAPOL in frozen solution yielded $T_{1e} = 554$ μs and $T_{2e} = 1.6$ μs.[26] For radicals in glassy organic solvents, the dominant relaxation mechanism of the electron spin is the second-order Raman process, which is independent of B^0.[27,26] Hence, the T_{1e} and T_{2e} values at $B^0 = 9.39$ T should be close to those determined at $B^0 = 3.35$ T. For $\tau_{\mu\mathrm{w}} = 120$ s, the FWHH in direct ^{29}Si spectrum is 440 Hz. Consequently the r distance must be longer than 3.0 nm for $S = 1/2$ or 3.5 nm for $S = 1$ according to Eq. S16.

References

[1] C. Song, K.-N. Hu, C.-G. Joo, T. M. Swager and R. G. Griffin, *J. Am. Chem. Soc.*, 2006, **128**, 11385–11390.

[2] L. J. Michot, I. Bihannic, K. Porsch, S. Maddi, C. Baravian, J. Mougel and P. Levitz, *Langmuir*, 2004, **20**, 10829–10837.

[3] A. Cadene, S. Durand-Vidal, P. Turq and J. Brendle, *J. Colloid Interface Sci.*, 2005, **285**, 719–730.

[4] B. A. Goodman, *Clay Miner.*, 1978, **13**, 351–356.

[5] P. L. Hall, *Clay Miner.*, 1980, **15**, 321–335.

[6] A. U. Gehring, I. V. Fry, T. Lloyd and G. Sposito, *Clays Clay Miner.*, 1993, **41**, 565–569.

[7] M. Rosay, L. Tometich, S. Pawsey, R. Bader, R. Schauwecker, M. Blank, P. M. Borchard, S. R. Cauffman, K. L. Felch, R. T. Weber, R. J. Temkin, R. G. Griffin and W. E. Maas, *Phys. Chem. Chem. Phys.*, 2010, **12**, 5850–5860.

[8] K.-N. Hu, *Prog. Nucl. Magn. Reson. Spectrosc.*, 2011, **40**, 31–41.

[9] B. M. Fung, A. K. Khitrin and K. Ermolaev, *J. Magn. Reson.*, 2000, **142**, 97 – 101.

[10] M. Lelli, D. Gajan, A. Lesage, M. A. Caporini, V. Vitzthum, P. Miéville, F. Héroguel, F. Rascón, A. Roussey, C. Thieuleux, M. Boualleg, L. Veyre, G. Bodenhausen, C. Copéret and L. Emsley, *J. Am. Chem. Soc.*, 2011, **133**, 2104–2107.

[11] O. Lafon, M. Rosay, F. Aussenac, X. Lu, J. Trébosc, O. Cristini, C. Kinowski, N. Touati, H. Vezin and J.-P. Amoureux, *Angew. Chem. Int. Ed.*, 2011, **50**, 8367–8370.

[12] D. G. Cory and W. M. Ritchey, *J. Magn. Reson.*, 1988, **80**, 128–132.

[13] J. H. Rayner and G. Brown, *Clays Clay Miner.*, 1973, **21**, 103–114.

[14] M. Morvan, D. Espinat, J. Lambard and T. Zemb, *Colloids and Surfaces A: Physicochemical and Engineering Aspects*, 1994, **82**, 193–203.

[15] H. J. M. Hanley, C. D. Muzny and B. D. Butler, *Langmuir*, 1997, **13**, 5276–5282.

[16] P. A. Wheeler, J. Wang, J. Baker and L. J. Mathias, *Chem. Mater.*, 2005, **17**, 3012–3018.

[17] S. Borsacchi, M. Geppi, L. Ricci, G. Ruggeri and C. A. Veracini, *Langmuir*, 2007, **23**, 3953–3960.

[18] I. Solomon, *Phys. Rev.*, 1955, **99**, 559–565.

[19] M. Gueron, *J. Magn. Reson.*, 1975, **19**, 58–66.

[20] G. Kervern, G. Pintacuda, Y. Zhang, E. Oldfield, C. Roukoss, E. Kuntz, E. Herdtweck, J.-M. Basset, S. Cadars, A. Lesage, C. Copéret and L. Emsley, *J. Am. Chem. Soc.*, 2006, **128**, 13545–13552.

[21] N. Bloembergen, *J. Chem. Phys.*, 1957, **27**, 572–573.

[22] J. Koehler and J. Meiler, *Prog. Nucl. Magn. Reson. Spectrosc.*, 2011, **59**, 360–389.

[23] I. Bertini, L. Emsley, M. Lelli, C. Luchinat, J. Mao and G. Pintacuda, *J. Am. Chem. Soc.*, 2010, **132**, 5558–5559.

[24] A. Abragam, *The Principles of Nuclear Magnetism*, Oxford University Press, Oxford, 1961.

[25] R. E. Connick and D. Fiat, *J. Chem. Phys.*, 1966, **44**, 4103–4107.

[26] A. Zagdoun, G. Casano, O. Ouari, G. Lapadula, A. J. Rossini, M. Lelli, M. Baffert, D. Gajan, L. Veyre, W. E. Maas, M. Rosay, R. T. Weber, C. Thieuleux, C. Copéret, A. Lesage, P. Tordo and L. Emsley, *J. Am. Chem. Soc.*, 2011, **134**, 2284–2291.

[27] A. Abragam and B. Bleaney, *Electron paramagnetic resonance of transition ions*, Oxford University Press, 1970.